Mechanics Research Communications 103 (2020) 103475

Contents lists available at ScienceDirect

Mechanics Research Communications

journal homepage: www.elsevier.com/locate/mechrescom

Effects of random disturbances on the stability of a temporally evolving incompressible plane wake

Bruno Jacob[a,*], Lucas Eduardo Ribeiro Duarte[b], João Rodrigo Andrade[c], Carlos Antonio Ribeiro Duarte[d]

[a] Department of Mechanical Engineering, University of California at Santa Barbara, Santa Barbara, CA 93106, USA
[b] Departament of Eletrical Engineering, Federal University of São Carlos, Rodovia Washington Luis, km 235, São Carlos, 13565-905, São Paulo, Brazil
[c] School of Mechanical Engineering, Federal University of Uberlândia, João Naves de Ávila Avenue, 2121, bloco 5P, Uberlândia, Minas Gerais, 38400-902 Brazil
[d] Department of Engineering, Federal University of Goiás - Regional Catalão, Dr. Lamartine Pinto de Avelar,Catalão, 1120, Goiás, Brazil

ARTICLE INFO

Article history:
Received 17 October 2019
Revised 8 January 2020
Accepted 9 January 2020
Available online 15 January 2020

Keywords:
DNS
LES
Temporal wake
Pseudospectral Fourier method
RFG

ABSTRACT

Direct Numerical Simulations (DNS) and Large Eddy Simulations (LES) of a three-dimensional, temporally evolving incompressible plane wake are performed, seeking to evidence differences in stability, transition and onset of both coherent and fine-scale structures arisen from random perturbations of different amplitudes. The perturbations are generated by the Random-Flow-Generator (RFG) technique, being imposed in the flow as initial conditions. The Navier-Stokes equations are solved in a prismatic domain with periodic boundary conditions in all directions, using a Fourier pseudospectral method. The invariants of the velocity gradient tensor were evaluated for cases with wakes subjected to random perturbations of amplitude 10^{-3}, 10^{-4} and 10^{-5}. Moreover, maps of the second and third invariants of the rate-of-strain tensor were analyzed, seeking to evidence the differences in local flow strain and topological characteristics of the dissipation of kinetic energy. In order to assess the fine-scale structures, isosurface plots of the *Q*-criterion, as well as vorticity contours were used, allowing visual identification of the coherent structures and confirming patterns predicted by the invariant maps. It was found that the characteristic teardrop correlation map is well defined for higher disturbance amplitudes. Based on the analysis of the simulation results, it can be concluded that the fluid element topology allowed a comparative study of the effects of perturbation amplitude on pairing mechanisms.

1. Introduction

Over the last decades, the study of free-shear flows is standing out among the classical transitional flow research, due to its physical importance and complexity. This important group of flows is characterized by the absence of walls and obstacles, although often their onset is related to the presence of flow past immersed bodies (wakes), expansion in nozzles (jets) and flows with two different streamwise velocities (mixing layers).

In particular, the turbulence in wakes has been widely investigated, both through numerical [1,2] and experimental [3–6] approaches, seeking for a better understanding of the mechanisms responsible for the onset of primary instabilities, and also for its degeneration into three-dimensional, fine-scale turbulent structures. One of the most important studies about the stability of turbulent wakes, the work of [3], provides a set of experimental results for a wake generated behind a thin flat plate. Their study allowed the classification of three different regions in the wake: a linear region, where the Kelvin-Helmholtz instabilities predominates and the amplitude disturbances grow exponentially; a nonlinear region, where the onset of von Kármán eddies occurs; and a three-dimensional region, mainly characterized by the presence of strong three dimensional motions. Since then, this classification has been used in several works, including the present paper.

Despite the advances in the understanding and prediction of motions in the linear wake region, there is still a lack of conclusive theories addressed to explain the stability characteristics of the nonlinear counterpart.

In this sense, the present paper proposes the usage of computational simulations to provide both qualitative and quantitative results, in order to scrutinize the mechanisms associated with the nonlinear and three-dimensional regions in wakes. Thus, this work provides a brief analysis on the transition and the onset of fine scale structures in a temporally evolving, incompressible plane

* Corresponding author.
E-mail address: bruno@engineering.ucsb.edu (B. Jacob).

https://doi.org/10.1016/j.mechrescom.2020.103475
0093-6413/

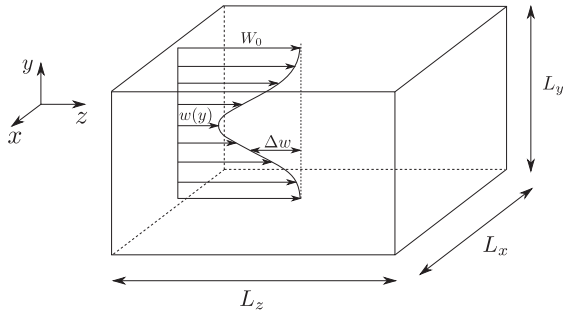

Fig. 1. Computational domain used in the simulations of the time-developing plane wakes, and initial Gaussian streamwise profile, based on [2,3,7].

Table 1
General setup (adopted in all cases).

Parameter	LES and DNS
Domain (x, y, z)	$20b \times 20b \times 40b$
Total simulation time	300[s]
CFL	0.8, 0.4
Velocity deficit, Δw	0.692
Reference velocity, w_o	1.0
Inflection constant, c	0.69315
Freestream velocity, W_0	1.0
Reynolds number, Re	346
Temporal integration scheme	RK46

wake at $Re = 346$. In order to understand the effects of different amplitude perturbations on dissipative scales and early coherent structures, we have undertaken computational simulations by solving the Navier-Stokes equations using a high-accuracy Fourier pseudospectral method.

2. Physical model

Typically, the development of a flow may occur by two different ways: under spatial or temporal development. The present work addresses a wake under temporal development, where the instabilities arise from a process of disturbance amplification, injected by external sources. Alternatively, it is possible to understand the temporal development as a Lagrangian framework, following the spatially-development flow in the streamwise direction.

The reason for choosing a temporal simulation lies on the fact that three-dimensional spatially evolving simulations are very expensive, in terms of computational time and memory, specially when dealing with DNS simulations. For temporal simulations, it is possible to choose a smaller domain, in order to capture far turbulence regions. Thus, the temporal simulation stands out as a viable option, taking advantage the periodicity in all directions, being a good match for Fourier pseudospectral methods.

The initial w-velocity profile simulated is shown in Fig. 1. The flow is confined in a prismatic region of lengths L_x, L_y, L_z, where x, y and z are the spanwise, cross-stream and streamwise directions, respectively.

Typically, in free-shear flow simulations, the velocity must be characterized by an inflectional profile, which usually shows abruptly growth, such as hyperbolic tangents and Gaussian profiles. The chosen profile was the same used by [1,2]:

$$w(x, y, z)|_{t=0} = w_o - \Delta w e^{-cy^2} \tag{1}$$

with w_o, Δw and c given by Table 1.

The remaining components, u and v, were considered identically zero for $t = 0$. Note that it is possible to decompose the velocity components as follows:

$$u(x, y, z)|_{t=0} = \overline{u} + a_u u', \tag{2}$$

$$v(x, y, z)|_{t=0} = \overline{v} + a_v v', \tag{3}$$

$$w(x, y, z)|_{t=0} = \overline{w} + a_w w', \tag{4}$$

where $\overline{u}, \overline{v}$ and $\overline{w}$ denote the mean velocity fields, and a_u, a_v, a_w are the amplitudes of the velocity fluctuations u', v', w'. The components u and v were initially chosen as zero, as well as their means $\overline{u} = \overline{v} = 0$.

The numerical experiment can only develop if some kind of disturbance is added to the flow. The transition process was shown to be highly dependent of initial disturbances [8], in such a manner that, if no fluctuation is added, and under conditions of a high-order or spectral solver being adopted, it is expected that transition does not occur.

In the present work, a recent random noise generator, the RFG method [9], was used. The main advantage of this model resides in its straightforward implementation, as well as its lower computational cost, when compared with other digital noise generators. This method allows the generation of mass conservative velocity fluctuations, with predetermined characteristic length and time scales, allowing one to reproduce experimental fluctuations in a computational environment. The complete list of features of the RFG can be found in [9].

3. Pseudospectral method

Note that a convolution term is obtained while applying the project tensor to transform the Navier-Stokes equations to the Fourier space. The solution of this term is imperative before proceeding with the evaluation of the primitive variables. However, the numerical solution of the convolution integral is impracticable, in terms of computational cost and time. An alternative to overcome this issue is to use a pseudospectral approach, on which the product is evaluated in the physical space and only after this step the resulting term is transformed to Fourier space. The main advantage of this approach is that it conserves the high-order and high-accuracy of the spectral method, avoiding the direct computation of the convolution product.

4. Turbulence modeling

Two different approaches were chosen to model the turbulence. For cases #1, 2 and 3, we performed direct numerical simulations, considering the scales of the problem and following the Kolmogorov theory. For the remaining cases (#4, 5 and 6), large-eddy simulations were performed, using the dynamic Smagorinsky model [10].

5. Cases description

5.1. Direct numerical simulations

The DNS approach is the most straightforward way to simulate turbulence. It consists in the attempt of resolving all the scales in the flow; i.e, from the largest (coherent) scales up to the smallest (dissipative) scales, without making usage of average or filtering operators in the velocity field. Thus, in order to perform DNS simulations, it is necessary to first estimate the order of magnitude of the dissipative scales in the flow. For this purpose, is is possible to define a local Reynolds number

For the DNS simulations, a characteristic time $t = 1.445[s]$, an initial halfwidth of $b = 1[m]$ and a $Re_b = 346$ were used. The required number of Fourier modes can be estimated based on the domain size. Strictly speaking, for the studied domain ($20b \times 20b \times 40b$), it would be necessary approximately

Table 2
Fluctuation amplitudes for each simulation case.

Case #	a_u, a_v, a_w	Turbulence model	Fourier modes
1	1×10^{-3}	DNS	$256 \times 256 \times 512$
2	1×10^{-4}	DNS	$256 \times 256 \times 512$
3	1×10^{-5}	DNS	$256 \times 256 \times 512$
4	1×10^{-3}	LES - D. Smag.	$128 \times 128 \times 256$
5	1×10^{-4}	LES - D. Smag.	$128 \times 128 \times 256$
6	1×10^{-5}	LES - D. Smag.	$128 \times 128 \times 256$

$1600 \times 1600 \times 3200$ Fourier modes, in order to capture all the scales in the flow and perform DNS in Kolmogorov theory sense. This number would make the simulations infeasible. However, the literature highlights that the Kolmogorov scales only estimate the dissipative scales [2]. In this sense, for cases #1, 2 and 3, the domain was divided in $256 \times 256 \times 512$ Fourier modes, resulting in a characteristic length approximately 6 times coarser than the Kolmogorov scales.

5.2. Large-eddy simulations

The large-eddy simulations were performed using the dynamic Smagorinsky subgrid model [11], allowing quantitative comparisons with the DNS simulations. In the dynamic model, the Smagorinsky constant C_s is replaced by a proportionality function $C_{sd}(\boldsymbol{x}, t)$, which is evaluated for each time step and for each discrete position in the domain. A summary of all the simulation cases is given in Table 2.

6. Topological analysis

In order to access the details of vortex dynamics in the temporal wakes, we evaluate and study the second and third invariants of the velocity gradient tensor. For a quantitative analysis, the approach of Refs. [2,12–14] were followed, using invariant maps to study the behavior of dissipative scales.

7. Results and discussions

7.1. Isosurfaces of Q

The following isosurfaces of Q were rendered in order to allow a visual identification on the differences in the temporal evolution, for cases #1,2 and 3. The quantitative results of cases #4, 5 and 6 have been omitted, given that only minor significant differences were observed, when compared with the DNS cases. The levels of Q were fixed in a range, in such a manner that $0 < Q < \max(Q)$, excluding possible hyperbolic structures (*i.e.*, levels where $Q < 0$) and thus following the definition of vortex proposed by Jeong and Hussain [15]. A slice of the central YZ plane, showing the vorticity magnitude, $|\boldsymbol{\omega}|$, is also provided in a perspective view. It is important to highlight that the derivatives needed for the numerical calculation of the Q, $|\boldsymbol{\omega}|$ and any other quantity expressed in this paper were evaluated using spectral accuracy.

Fig. 2 shows the temporal evolution of the isosurfaces of Q for case #1 (*c.f.* Table 1). It was possible to distinguish two different pairing mechanisms acting on the coherent structures, along different stages in the development of the wake. The first mechanism, here denoted by *primary pairing mechanism*, can be seen in Figs. 2-(a) (azimuth view) and 3 (top view). On these figures, it is possible to notice the presence of structures endowed with strong coherence, in the form of rolls, called Kelvin-Helmholtz instabilities.

It is also noticeable that some of these coherent structures show higher curvatures than others. Note that one of the Kelvin-Helmholtz (*c.f.* Fig. 3) has a sharp curvature, high enough to allow

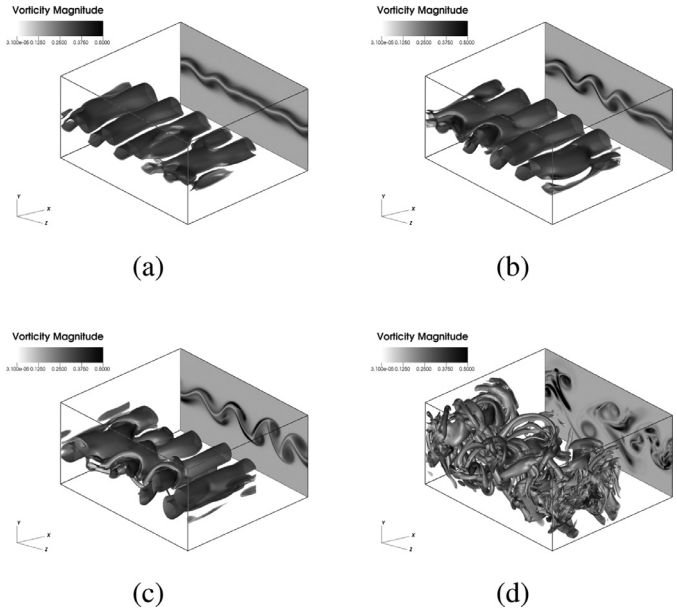

Fig. 2. Isosurfaces of Q, colored by vorticity magnitude $|\boldsymbol{\omega}|$ (front) and slice of central YZ plane, showing contours of $|\omega|$ (back), for a disturbance amplitude of 10^{-3}, for (a) $t = 135[s]$, (b) $t = 165[s]$, (c) $t = 195[s]$ and (d) $t = 270[s]$.

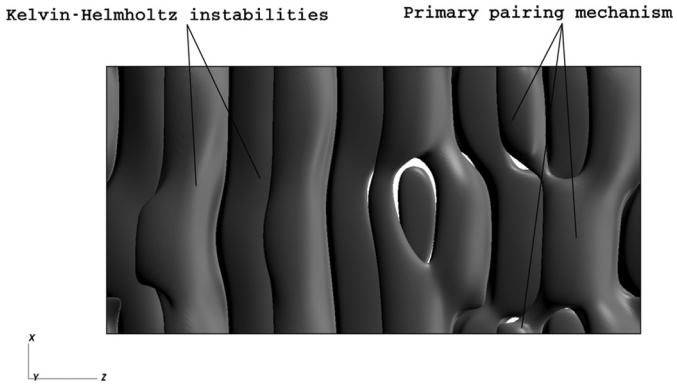

Fig. 3. Evidence of primary pairing mechanism, acting in the Kelvin-Helmholtz instabilities, viewed from the top (XZ plane), for a disturbance amplitude of 10^{-3}, for $t = 135[s]$.

the pairing with the structure immediately preceding to it, resulting in a reticulated structure, composed of two Kelvin-Helmholtz structures.

Another important result is also observed in Figs. 2-(b) and 4. The hairpin vortices appear to interlace the Kelvin-Helmholtz instabilities, causing a mechanical effect of stretching on these longitudinal rolls. Such pairing mechanism appears to occur due to differences in the advection of the Kelvin-Helmholtz instabilities, which is strongly influenced by the external disturbances imposed on the flow. This mechanism, therefore, acts as a *secondary pairing mechanism*, originating counter-rotating structures called von Kármán eddies. This mechanism plays an important role in the development of the wakes, since the onset of von Kármán eddies characterizes the beginning of the nonlinear growth region.

Figs. 2 -(c) and 5 reveal that the displacement of the coherent structures, subjected to different shear stresses and local velocities, cause distortions in the reticulated structures formed by the primary pairing mechanism. This effect, in turn, causes the degeneration of the hairpin vortices observed in Figs. 2-(b) and 4, due to the stretching in the longitudinal filaments. Finally, Figs. 2-(d) and 6 show a later stage on the development of the secondary pairing

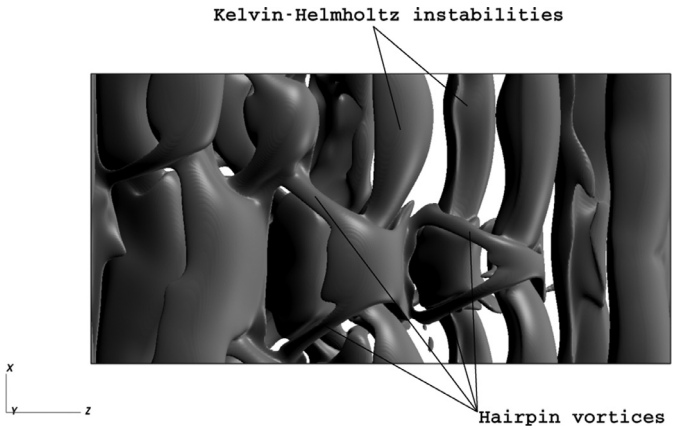

Fig. 4. Pattern of hairpin vortices on the early evolution wake viewed from the top (*XZ* plane), generated by the primary pairing mechanism, for a disturbance amplitude of 10^{-3}, for $t = 165[s]$.

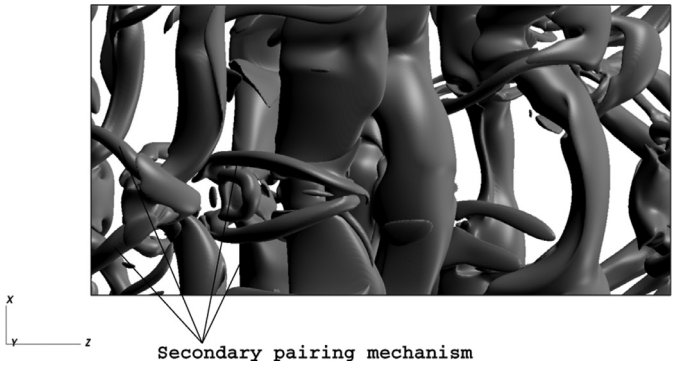

Fig. 5. Detail of the secondary pairing mechanism, viewed from top (*XZ* plane), showing the mechanical effect that the hairpin vortices exert in a pair of Kelvin-Helmholtz instabilities, for a disturbance amplitude of 10^{-3}, for $t = 180[s]$.

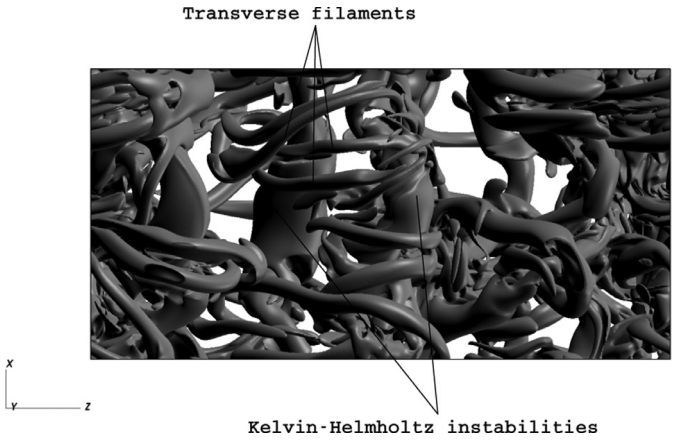

Fig. 6. Secondary pairing mechanism, in an advanced stage, viewed from top (*XZ* plane), for a disturbance amplitude of 10^{-3}, for $t = 270[s]$, showing the degeneration of hairpin vortices in three-dimensional filaments.

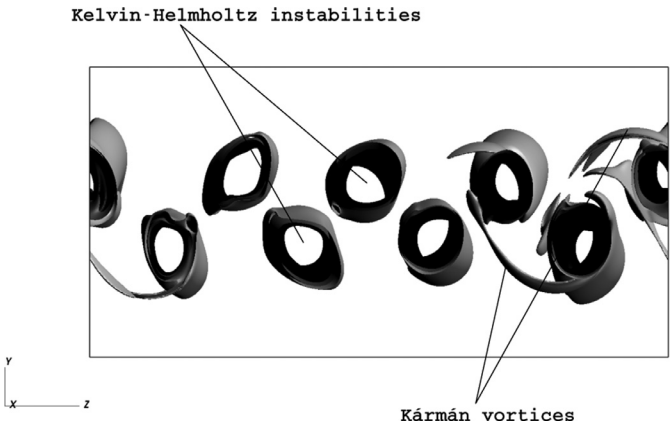

Fig. 7. Side view (*YZ* plane) of the wake, the Kelvin-Helmholtz instabilities, and the onset of Kármán vortices, due to the arise of instabilities in the spanwise direction. Disturbance amplitude of 10^{-5}, for $t = 300[s]$

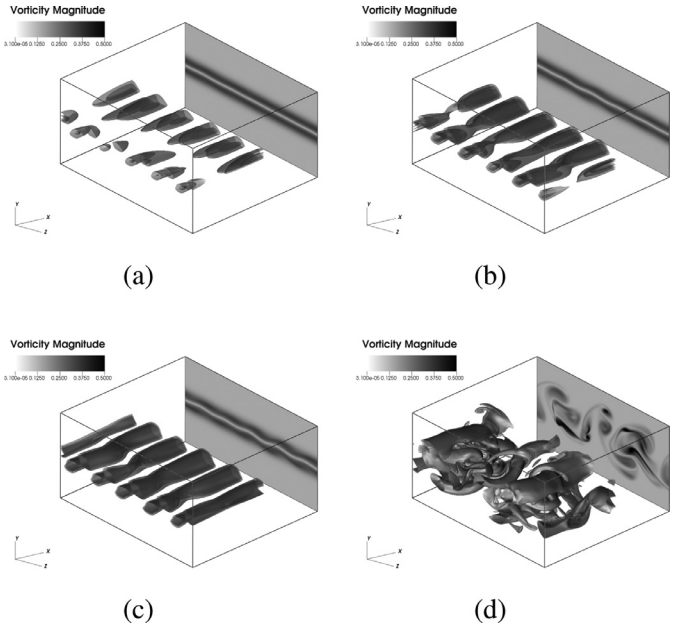

Fig. 8. Isosurfaces of *Q*, colored by vorticity magnitude $|\boldsymbol{\omega}|$ (front) and slice of central *YZ* plane, showing contours of $|\omega|$ (back), for a disturbance amplitude of 10^{-4}, for (a) $t = 135[s]$, (b) $t = 165[s]$, (c) $t = 195[s]$ and (d) $t = 270[s]$.

mechanism. At this stage, the hairpin vortices have already degenerated into longitudinal filaments and these structures predominate in the flow. Hence, it is possible to state that the wake has reached its three-dimensional stage.

A closer look at Figs. 2–9 permits to assess the qualitative effect caused by the different random perturbation amplitudes in the wake development. The strong coherence of the Kelvin-Helmholtz instabilities in cases #1, 2 and 3 remains in the roll-like shape over the time. In case #1, it is possible to infer that the 10^{-3} disturbance amplitude saturates the two-dimensional modes faster than observed for the 10^{-4} (case #2) and 10^{-5} (case #3) amplitudes. For this reason, case #2 presents a less intense energy state than observed in case #1. Comparing cases #1 and 2 at the same time ($t = 195[s]$), it is possible to see a strong presence of longitudinal filaments in the first (Fig. 2), while in the second (Fig. 8) the wake is still in its linear stage, with no significant three-dimensional motion.

The isosurfaces of *Q* for case #3 stands out as the one with the lowest energy state among all DNS cases. Notice that the saturation of the linear stage takes longer, when compared with the other cases, and therefore, the first von Kármán eddies are only visible at the last time step ($t = 300[s]$). Finally, Fig. 7 shows a side view of the wake in case #3, at $t = 300[s]$. The absence of strong three-dimensional motions and the secondary pairing mechanism acts between the Kelvin-Helmholtz instabilities, generating the longitudinal filaments that compose a pair of von Kármán eddies. This snapshot also shows that the wake of case #3 has reached

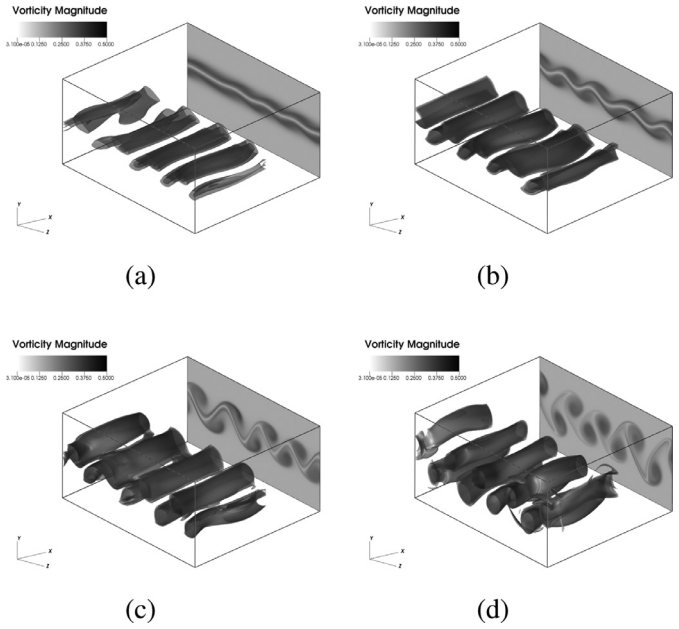

Fig. 9. Isosurfaces of Q, colored by vorticity magnitude $|\boldsymbol{\omega}|$ (front) and slice of central YZ plane, showing contours of $|\omega|$ (back), for a disturbance amplitude of 10^{-5}, for (a) $t = 210[s]$, (b) $t = 240[s]$, (c) $t = 270[s]$ and (d) $t = 300[s]$.

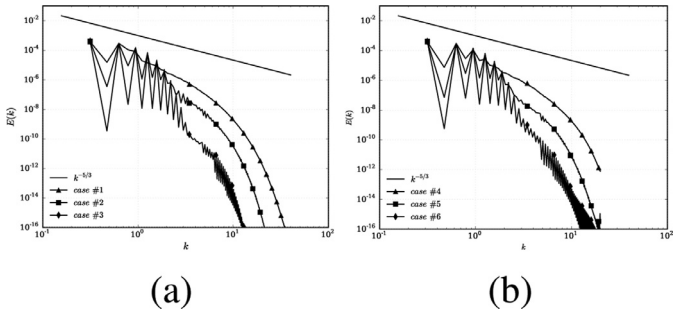

Fig. 10. Turbulent kinetic energy spectra for (a) DNS and (b) LES cases, for $t = 150[s]$

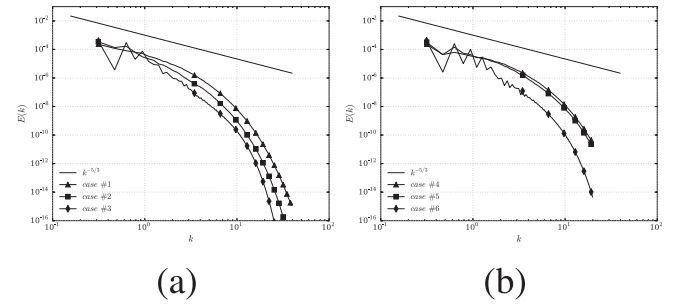

Fig. 11. Turbulent kinetic energy spectrum for (a) DNS and (b) LES cases, for $t = 240[s]$

the nonlinear stage in a later time step, when compared with cases #1 and 2.

7.2. Turbulent kinetic energy spectra

The turbulent kinetic energy spectra were calculated for all the simulated cases, using the three velocity components and its complex conjugates, both evaluated in Fourier space. It is clear from Figs. 10 and 11 that for the studied Reynolds number ($Re = 346$), the simulations did not achieve a fully developed turbulent regime,

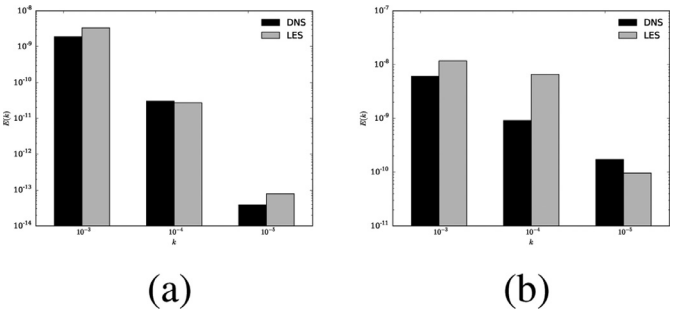

Fig. 12. Comparison between the energy levels $E(k)$ of the DNS and LES simulations, for $k = 10$, at (a) $t = 150[s]$ and (b) $t = 240[s]$.

as observed by Moser and Rogers [1]. However, it is noticed that the higher disturbance amplitudes caused a tendency of approximation to the Kolmogorov $-5/3$ slope.

In general, the turbulent kinetic energy spectra of the LES simulations (cases #4, 5 and 6) agreed well with the results from the DNS simulations. Moreover, the results showed a very clean dropoff at high wavenumbers.

Figs. 12 -(a) and (b) reveals the differences between the turbulent kinetic energy levels, for the DNS and LES cases at a fixed wavenumber in the decay region ($k = 10$), at the instants $t = 150[s]$ and $t = 240[s]$, respectively. This analysis allows a quantitative comparison of the energy level in the LES simulations against the DNS results. Such comparison permits one to check if the Dynamic Smagorinsky model has adequately modeled the fine-scale structures and/or has caused any accumulation of energy at this specific wavenumber. Figs. 12-(a) shows that, for the 10^{-3} and 10^{-5} cases, there was a small accumulation of turbulent kinetic energy in the LES simulations. This is also observed at the instant $t = 240[s]$ (Fig. 12-(b)), for the disturbance amplitudes of 10^{-3} and 10^{-4}.

7.3. Topological analysis

The following subsections provide a topological analysis of the fine-scale structures in the previous simulation cases. Scatter plots of Q *vs.* R, $-Q_S$ *vs.* Q_W and Q_S *vs.* R_S are shown and their physical interpretations are described.

7.3.1. Invariant maps of Q vs. R

The invariance maps of Q *vs.* R showed in the present work were constructed using the current values of these properties at each Fourier mode belonging to the central YZ plane. For this purpose, only the DNS simulations were considered (cases #1, 2 and 3), given that these results showed richer details than the LES simulations (cases #4, 5 and 6). In possession of these values, scatter plots were constructed for each time step considered.

The main features observed in the (Q, R) map for case #1 (Fig. 13) agreed with those observed by several authors (see Refs. [2,14,16]). At a three-dimensional stage of development, the collection of points lies predominantly in the upper left and lower right quadrants, forming a classical shape, usually referred in the literature as *teardrop* [2,16]. This shape was already observed in several types of turbulent flows [16], including isotropic turbulence, channel flows [17], compressible [12] and incompressible [2,14] shear flows. Moreover, preliminary results indicate that this shape seems to be strictly related with the solution of the Navier-Stokes equations, supporting the theory that this shape might be universal [14].

Still in Fig. 13, notice that the points tend to align along the region of $D = 0$ in the lower right quadrant. Fluid elements lying on this region tend to dissipate high levels of kinetic energy. From

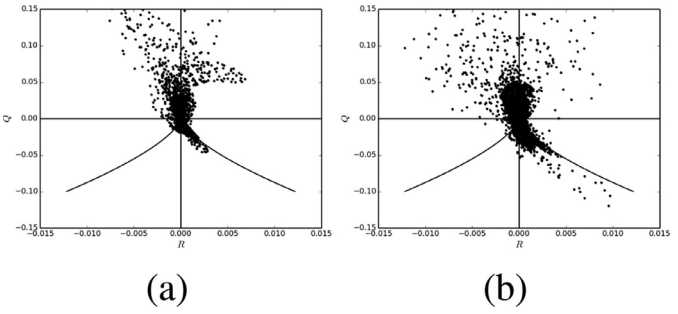

Fig. 13. Scatter plots of Q *vs* R, for a disturbance amplitude of 10^{-3}, for (a) $t = 180[s]$ and (b) $t = 240[s]$.

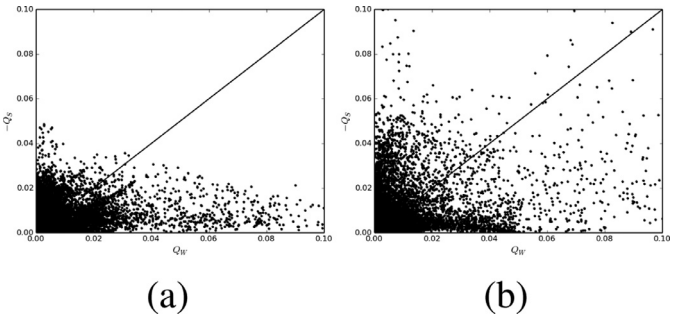

Fig. 14. Scatter plots of $-Q_S$ *vs* Q_W, for a disturbance amplitude of 10^{-3}, for (a) $t = 180[s]$ and (b) $t = 240[s]$.

Fig. 13-(a) to (b), it seems that more points migrate to this particular region, which agrees with the qualitative results provided. This increase of dissipative structures might be explained by the increasing of three-dimensional filaments in the flow.

7.3.2. Invariant maps of $-Q_S$ vs. Q_W

These invariant maps are specially useful for the topological analysis related with the dissipation of kinetic energy [16]. Fig. 14 shows the temporal evolution of the wake simulated in case #1. For $t = 180[s]$, a large number of points lie closer to the horizontal region, representing structures in which the enstrophy density is considerably higher than the dissipation, as it occurs outside of the vortex tubes [14]. Such phenomenon, in which the shape is similar to a half ellipsoid, is often observed in strongly three-dimensional flows [2] and agrees with the qualitative results previously showed. The strong dominance of three-dimensional filaments are originated from the secondary pairing mechanism, due to interactions between the hairpin vortices and the Kelvin-Helmholtz instabilities.

In the scatter plot shown in Fig. 14, for $t = 240[s]$, the topology in the invariant space has approximated to a L-shape scatter. This shape was reported by Sondergaard et al. [2] to be usual in flows which the turbulent motions have not reached the fully development stage.

7.3.3. Invariant maps of Q_S vs. R_S

These invariant maps provide a more detailed analysis of regions with intense kinetic energy dissipation, as well as the geometry behavior of the local deformation of the structures. As observed by previous works [2,14,18], it is possible to identify for the most perturbed simulations (Figs. 15,16, 17) that the structures show a preferred orientation towards the lower right quadrant ($R_S > 0$ and $Q_S < 0$), tending to align to the positive branch of the rate-of-strain discriminant, ($D_S = 0$). Therefore, the mean flow geometry is associated with the expansion of fluid elements [16]. Despite this supposed orientation preference, note that some few points also lie on the contraction region ($R_S < 0$).

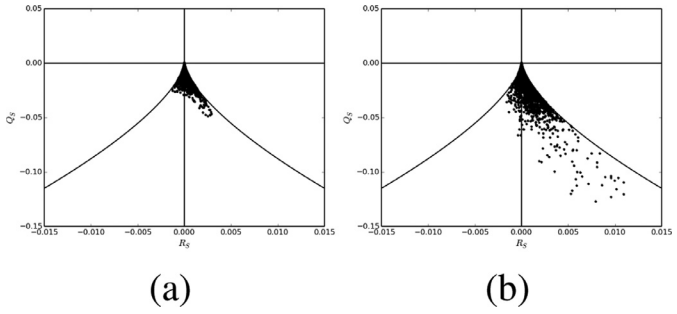

Fig. 15. Scatter plots of Q_S *vs* R_S, for a disturbance amplitude of 10^{-3}, for (a) $t = 180[s]$ and (b) $t = 240[s]$.

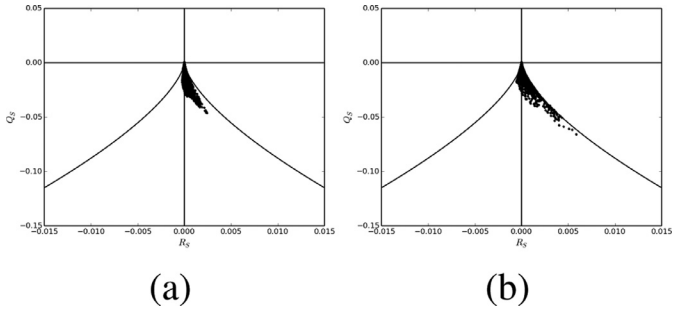

Fig. 16. Scatter plots of Q_S *vs* R_S, for a disturbance amplitude of 10^{-4}, for (a) $t = 180[s]$ and (b) $t = 240[s]$.

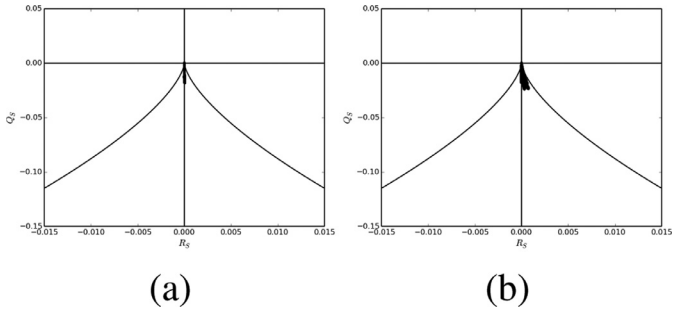

Fig. 17. Scatter plots of Q_S *vs* R_S, for a disturbance amplitude of 10^{-5}, for (a) $t = 180[s]$ and (b) $t = 240[s]$.

The points provided in Fig. 16-(a), for $t = 180[s]$ lie about the $Q_S = 0$ region, which means that an initial two-dimensional flow geometry is observed. This result can be justified considering the fact that the wake is still in its linear region (*c.f.* Fig. 8), *i.e.,* the linear stage is not saturated yet. However, despite the fact that the wake is still in its linear region, the fluid elements start to be subject to stretching mechanisms (*i.e.,* expansion). This phenomenon might be explained by the stretching in the coherent structures caused by the secondary pairing mechanism. Conversely, Fig. 16-(b) shows that the saturation already took place for $t = 240[s]$, since the points are much more aligned with the right branch of the $D_S = 0$ curve. This indicates that the axysimmetric expansion occurs in most part of the flow and might be explained by the stretching of longitudinal filaments due to the effects of the second pairing mechanism in an advanced stage, as showed in Fig. 6.

8. Conclusions

DNS and LES simulations of a turbulent wake were performed, subjected to three different random disturbances, imposed as ini-

tial conditions. The quantitative analysis allowed the comparison of how efficient the vorticity can be as vortex identification tool, when compared with the second invariant of the velocity gradient tensor, Q. It was shown that the vorticity tends to identify less accurately the vortical structures of a temporal wake in its early evolution stages, and for these purposes, the utilization of the Q criterion is strongly recommended.

The development of each disturbance amplitude case along the time were provided, evidencing the relation between different disturbance amplitudes and the time needed for transition and for the degeneration of coherent structures in three-dimensional, fine-scale structures. Early coherent structures were highlighted, and two different pairing mechanisms were identified and discussed. In terms of quantitative results, the turbulent kinetic energy spectra of all simulations for a specific time was shown, seeking for comparisons of LES and DNS cases. Scatter plots of invariant quantities were compared, allowing a physical interpretation on the stages of fine scale structures and correlations of the enstrophy density and local viscous dissipation of kinetic energy. A brief analysis of the fluid elements topology allowed a comparative study of the effects of the pairing mechanisms, identified in the qualitative results, with the invariant quantities.

Recently, advances in turbulence modeling, such as the finite scale theory and the implicit large eddy simulation (ILES) emerged to make mathematically more precise the role of the observer in the classical physics of fluid flows [19]. Additionally, the reader is referred to [20–24] for general references on these topics. These are in the scope of this work and will be studied in the future. We envision that implicit turbulence modeling approaches can be the key to answer many open questions related to other physical theories and numerical methods in fluid dynamics, including a more efficient coupling of turbulence models and spectral methods.

Declaration of interests

The authors declare that they have no known competing financial interests or personal relationships that could have appeared to influence the work reported in this paper.

Acknowledgments

The authors acknowledge the support given by the Coordination of Superior Level Staff Improvement (CAPES), Fundação de Amparo à Pesquisa do Estado de São Paulo (FAPEG), Fundação de Amparo à Pesquisa do Estado de Minas Gerais (FAPEMIG) and Fundação de Amparo à Pesquisa do Estado de Goiás (FAPEG) to this research.

References

[1] R.D. Moser, M.M. Rogers, Direct simulation of a self-similar plane wake, in: AGARD Symp. on App. of DNS and LES, Chania, Crete, Greece, 1994, pp. 248–255.
[2] R. Sondergaard, B. Cantwell, N. Mansour, Direct numerical simulation of a temporally evolving incompressible plane wake: effect on initial conditions on evolution and topology, Technical Report, NASA Ames Research Center, Stanford, CA, 1997.
[3] H. Sato, K. Kuriki, The mechanism of transition in the wake of a thin flat plate placed parallel to a uniform flow, J. Fluid Mech. 11 (03) (1961) 321–352.
[4] A.A. Townsend, Entrainment and the structure of turbulent flow, J. Fluid Mech. 41 (01) (1970) 13–46.
[5] D.R. Ko, T. Kubota, L. Lees, Finite disturbance effect on the stability of a laminar incompressible wake behind a flat plate, J. Fluid Mech. 40 (2) (1970) 315–341.
[6] H. Sato, H. Saito, Artificial control of the laminar-turbulent transition of a two-dimensional wake by external sound, J. Fluid Mech. 84 (04) (1978) 657–672.
[7] J.H. Chen, B.J. Cantwell, N.N. Mansour, The effect of Mach number on the stability of a plane supersonic wake, Phys. Fluids A 2 (6) (1990) 984.
[8] H. Maekawa, N.N. Mansour, J.C. Buell, Instability mode interactions in a spatially developing plane wake, J. Fluid Mech. 235 (1992) 223–254.
[9] A. Smirnov, S. Shi, I. Celik, Random flow generation technique for large eddy simulations and particle-dynamics modeling, J. Fluids Eng. 123 (2001) 359.
[10] J. Smagorinsky, Generical circulation experiments with the primitive equations, Month/ Weather Rev. 91 (3) (1963) 99–164.
[11] M. Germano, U. Piomelli, P. Moin, W.H. Cabot, A dynamic subgrid-scale eddy viscosity model, Phys. Fluids 1760 (1991) (1990).
[12] M.S. Chong, A.E. Perry, B.J. Cantwell, A general classification of three-dimensional flow fields, Phys. Fluids A 2 (1990) (1990) 765–777.
[13] B.J. Cantwell, The geometry of turbulent fine scale structure, in: 11th Australasian Fluid Mechanics Conference, Hobart, Australia, 1992, pp. 399–402.
[14] J. Soria, R. Sondergaard, B.J. Cantwell, M.S. Chong, A.E. Perry, A study of the fine-scale motions of incompressible time-developing mixing layers, Phys. Fluids 6 (1994) (1994) 871.
[15] J. Jeong, F. Hussain, On the identification of a vortex, J. Fluid Mech. 285 (1995) 69–94.
[16] C.B. Silva, J.C.F. Pereira, Invariants of the velocity-gradient, rate-of-strain, and rate-of-rotation tensors across the turbulent/nonturbulent interface in jets, Phys. Fluids 20 (May) (2008) 1–18.
[17] H.M. Blackburn, N.N. Mansour, B.J. Cantwell, Topology of fine-scale motions in turbulent channel flow, J. Fluid Mech. 310 (1996) 269.
[18] C.B. Silva, O. Metais, Vortex control of bifurcating jets: a numerical study, Phys. Fluids 14 (11) (2002) 3798–3819.
[19] L. Margolin, Finite scale theory: The role of the observer in classical fluid flow, Mech. Res. Commun. 57 (2014) 10–17.
[20] L.G. Margolin, P.K. Smolarkiewicz, Z. Sorbjan, Large-eddy simulations of convective boundary layers using nonoscillatory differencing, Phys. D 133 (1) (1999) 390–397.
[21] L.G. Margolin, P.K. Smolarkiewicz, A.A. Wyszogradzki, Dissipation in implicit turbulence models: a computational study, J. Appl. Mech 73 (3) (2006) 469–473.
[22] L.G. Margolin, M. Shashkov, Finite volume methods and the equations of finite scale: a mimetic approach, Int. J. Numer. Method. Fluids 56 (8) (2008) 991–1002.
[23] L.G. Margolin, M. Shashkov, Mpdata: gauge transformations, limiters and monotonicity, Int. J. Numer. Method. Fluids 50 (10) (2006) 1193–1206.
[24] L.G. Margolin, W.J. Rider, The design and construction of implicit les models, Int. J. Numer. Method. Fluids 47 (10–11) (2005) 1173–1179.